



### Science Arts & Métiers (SAM)

is an open access repository that collects the work of Arts et Métiers Institute of Technology researchers and makes it freely available over the web where possible.

This is an author-deposited version published in: <https://sam.ensam.eu>  
Handle ID: <http://hdl.handle.net/10985/24902>



This document is available under CC BY license

#### To cite this version :

Liza EL-KHOURY, Nathalie DARO, Guillaume CHASTANET, Patrick ROSA, Dominique DENUX, Laetitia ETIENNE, Vincent MAZEL, Michaël JOSSE, Mathieu MARCHIVIE - Spin crossover molecular ceramics by Cool-SPS: consequences on switching features beyond the sole microstructural effect - Materials Advances - Vol. 5, n°4, p.1502-1512 - 2024

Any correspondence concerning this service should be sent to the repository

Administrator : [scienceouverte@ensam.eu](mailto:scienceouverte@ensam.eu)



# Materials Advances

Accepted Manuscript

This article can be cited before page numbers have been issued, to do this please use: L. El-Khoury, N. Daro, G. Chastanet, P. Rosa, D. Denux, L. Etienne, V. Mazel, M. Josse and M. Marchivie, *Mater. Adv.*, 2023, DOI: 10.1039/D3MA00688C.



This is an Accepted Manuscript, which has been through the Royal Society of Chemistry peer review process and has been accepted for publication.

Accepted Manuscripts are published online shortly after acceptance, before technical editing, formatting and proof reading. Using this free service, authors can make their results available to the community, in citable form, before we publish the edited article. We will replace this Accepted Manuscript with the edited and formatted Advance Article as soon as it is available.

You can find more information about Accepted Manuscripts in the [Information for Authors](#).

Please note that technical editing may introduce minor changes to the text and/or graphics, which may alter content. The journal's standard [Terms & Conditions](#) and the [Ethical guidelines](#) still apply. In no event shall the Royal Society of Chemistry be held responsible for any errors or omissions in this Accepted Manuscript or any consequences arising from the use of any information it contains.

## ARTICLE

## Spin Crossover Molecular Ceramics by Cool-SPS: Consequences on Switching Features Beyond the sole Microstructural effect.

Liza El-Khoury,<sup>a</sup> Nathalie Daro,<sup>a</sup> Guillaume Chastanet,<sup>a</sup> Patrick Rosa,<sup>a</sup> Dominique Denux,<sup>a</sup> Laetitia Etienne,<sup>a</sup> Vincent Mazel,<sup>b</sup> Michael Josse<sup>\*a</sup> and Mathieu Marchivie<sup>\*a</sup>.Received 00th January 20xx,  
Accepted 00th January 20xx

DOI: 10.1039/x0xx00000x

The sintering of spin crossover material using Spark Plasma Sintering at low temperature (Cool-SPS) lead to a new way of shaping such compounds into functional molecular ceramics. These ceramics reach a high relative density of 95%, what may address several issues for using spin crossover materials into barocaloric devices. Starting from the reference complex  $[\text{Fe}(\text{Htrz})_2(\text{trz})]\text{BF}_4$ , we first investigated the magnetic, structural, microstructural properties as well as the fatigability behavior of the starting powder using multiple magnetic measurements, X-ray diffraction and calorimetry to compare them to the elaborated ceramics. The best conditions of pressure and temperature during the SPS process to obtain reproducible molecular ceramics with high relative density where found to be between 250 and 300 °C, and 300 and 400 MPa. The same complete set of characterizations made on a molecular ceramic of 95% of relative density reveal that crystal structure as well as the abrupt hysteretic SCO of  $[\text{Fe}(\text{Htrz})_2(\text{trz})]\text{BF}_4$  are perfectly conserved after sintering. However, ceramic presents a faster stabilization of their microstructural and magnetic properties upon cycling and a higher cooperativity at the macroscopic level was observed compared to the starting powder.

## Introduction.

Ceramics have been widely used since antiquity to form ores and compounds into functional materials. Nowadays, ceramics are probably one of the most used form to shape and investigate solids into functional materials. They are present in numerous high technology applications such as microelectronics and are widely studied to design smart materials in the emergent green economy through energy storage application, solar cell or caloric materials.<sup>1–4</sup> Ceramics are mainly based on tough compounds such as inorganic metal oxides. Fragile and low density materials, on the other hand, are very scarcely elaborated as ceramics, despite a great interest, mainly due to their limited thermal stability preventing application of conventional sintering processes. During the last decade however, low temperature sintering methods started to grow<sup>5–8</sup> and very recently ceramics of thermodynamically fragile materials were obtained by Cool-SPS<sup>9–11</sup> (low temperature SPS, where SPS = Spark Plasma Sintering), leading to the conception of dense and cohesive polycrystalline molecular materials, i.e. *molecular ceramics*. While the sintering process is not fully understood,<sup>10</sup> this novel approach opens a

new way for shaping into ceramics compounds belonging to the very wide and versatile world of functional molecular materials. Among them, molecular switches constitute a promising class of materials that can be switched between two or more different states upon an external stimulus. Due to their high versatility their interest keeps growing in the scientific community owing to numerous potential applications like memories, sensors, molecular motors, actuators or quantum materials.<sup>12–16</sup> Spin CrossOver (SCO) complexes represent one of the very promising families of such molecular switches where the switching states, separated by a small energy gap, correspond to two different electronic configurations with distinct spin repartitions.<sup>17–22</sup> Considering octahedral complexes of  $\text{Fe}^{2+}$  cation, which represent the most reported cases, the two configurations correspond to a low spin state (LS) of electronic configuration  $t_{2g}^6e_g^0$  ( $S=0$ ) and a high spin state (HS) of electronic configuration  $t_{2g}^4e_g^2$  ( $S=2$ ). The crossover between these two states can be triggered by numerous stimuli such as temperature, pressure, magnetic field, light irradiation, electric field<sup>23–28</sup> or chemical sorption...<sup>29–31</sup> The SCO signature can be probed by several physical properties changes such as magnetic susceptibility, optical measurements, vibrational spectroscopies, structural changes,<sup>32</sup> thermodynamic properties<sup>33</sup> and more scarcely studied changes in conductivity or dielectric constant.<sup>34–36</sup> These last effects may be very interesting concerning potential applications in electronic devices but require difficult measurements on single crystal, compressed powders or thin layers. Due to the high versatility of their possible chemical composition and their wide structural diversity, SCO materials

<sup>a</sup> Univ. Bordeaux, CNRS, Bordeaux INP, ICMCB, UMR 5026, F-33600 Pessac, France, Email : mathieu.marchivie@icmcb.cnrs.fr; michael.josse@icmcb.cnrs.fr

<sup>b</sup> Univ. Bordeaux, CNRS, I2M Bordeaux, 146 rue Léo Saignat, F-33000 Bordeaux, France

Electronic Supplementary Information (ESI) available: [Additional information such as sintering maps, diametral compression test of pellets, and complementary figures can be found in an additional pdf file.]. See DOI: 10.1039/x0xx00000x





show very wide panel of switching behaviours from gradual to very abrupt transitions with or without hysteresis loop. Besides, the salient role of the crystal structure on SCO feature is now well established.<sup>32,37,38</sup> Notably, intermolecular interactions have been widely studied and the key role of hydrogen bonding network, pi-pi stacking<sup>39</sup> or even H-H Van Der Waals contacts has been proved to play a crucial role on cooperativity and hysteresis loops width.<sup>40,41</sup> Beyond the crystal structure, the shaping of SCO complexes was investigated for several years to form nanomaterials<sup>19,42</sup>, thin or thick films,<sup>43,44</sup> submonolayers,<sup>45,46</sup> composites with polymers...<sup>47</sup> Most of these material forms lead to modification of the SCO features, what shed light on the multiscale nature of the SCO properties and triggered new approaches of this phenomenon.<sup>48</sup> From atoms, to bonds, to coherent domains, links were established that related macroscopic features of SCO to the contributions of the aforementioned microscopic phenomena. However, throughout the various characteristic scales of materials, the influence of the microstructure, with features such as grain boundaries, is less investigated may be due to the lack of controlled ways to modify microstructural characteristics in molecular systems. Molecular ceramics could contribute to address this issue. Additionally, SCO materials have been recently identified as very promising systems for barocaloric applications provided overcoming their low density and low thermal conductivity.<sup>49,50</sup> Shaping SCO compounds into ceramics could address these concerns. Nevertheless, although ceramics are ubiquitous in solid state chemistry, it is worth to note that ceramics were almost never explored concerning molecular compounds and SCO materials have never been elaborated as ceramics to date.

The aim of this communication concerns the preparation of a ceramic of a SCO coordination polymer by Cool-SPS and the investigation of its impact onto the functional property. We chose the well-known  $[\text{Fe}(\text{Htrz})_2(\text{trz})](\text{BF}_4)$  complex (where Htrz = 1H-1,2,4-triazole) as starting material because of its well-controlled synthesis route, its wide hysteresis loop above room temperature and its good stability till ca. 300 °C. Additionally, microstructural effects have been already studied on this compound at the nanoscale,<sup>42,51–54</sup> after integration in a polymer matrix,<sup>55,56</sup> under hydrostatic pressure<sup>57,58</sup> or during grinding experiments suggesting a possible dependence of the SCO features upon shaping.<sup>59,60</sup>

We propose here to explore the effect of sintering of  $[\text{Fe}(\text{Htrz})_2(\text{trz})](\text{BF}_4)$  on the structural, microstructural and SCO features by comprehensive comparison between powder and molecular ceramics obtained by Cool-SPS.

## Experimental section

**Synthesis procedure of  $[\text{Fe}(\text{Htrz})_2(\text{trz})](\text{BF}_4)$  (1).** All the chemicals and solvents were used as purchased. The iron salt ( $\text{Fe}(\text{BF}_4)_2 \cdot 6\text{H}_2\text{O}$ ; 97 %), the triazole (1H-1,2,4-triazole, 98 %) and the ascorbic acid (99 %) were used.

The synthesis consists in first dissolving the iron salt ( $\text{Fe}(\text{BF}_4)_2 \cdot 6\text{H}_2\text{O}$ ) (3 mmol) with few mg of ascorbic acid into 5 mL of demineralized water on one side and the triazole (1H-1,2,4-

triazole, Htrz) (9 mmol) into 5 mL of ethanol on the other side. The two solutions were heated at 80 °C. Then, the solution of Htrz was added dropwise to the iron solution with magnetic stirring at 80 °C under  $\text{N}_2$  atmosphere. The two solutions were let to react with mixing during 15 min at 80 °C. The resulting purple suspension was then let to cool down at 5 °C during 1 hour to promote precipitation. After centrifugation (12 000 rcf, 5 minutes) of the suspension, the precipitate was washed three times with ethanol and once with diethyl ether (50 mL of solvent was used each time). For these washing steps, the precipitate was separated from the solvent by the same procedure of centrifugation. The precipitate was finally let to dry at RT under ambient atmosphere overnight and a purple powder was obtained.

**Sintering by Cool-SPS.** A SPS machine (Dr Sinter SPS-515S) operating under vacuum ( $P \approx 10$  Pa) was used. To allow for application of large pressures (up to 600 MPa), a Tungsten Carbide (WC) mould was used. To protect both the sample and the mould, a carbon foil (Papyex®) of 0.2 mm thickness separated them. Approximately 200 mg of starting powder were used to elaborate a ceramic. Once prepared, the die assembly containing the powder was placed in the SPS chamber, which was evacuated, and the selected sintering sequence was subsequently applied, using a 12:2 pulse sequence. Throughout the sintering, several instrumental parameters were monitored including voltage, current, temperature, applied force, SPS chamber pressure and displacement. Cold-pressing experiment were run in the SPS environment without application of any electrical power, thus using the same die and applying the pressure in an identical way. Samples were recovered by dismounting the three-parts mould, to preserve the integrity of obtained ceramics.

**X-Ray diffraction.** Powder X-ray diffraction (PXRD) patterns were collected on a PANalytical X'pert PRO MPD diffractometer in Bragg-Brentano  $\theta$ -2 $\theta$  geometry equipped with a primary monochromator (oriented Ge(111) crystal) to filter the  $\text{K}\alpha_2$  radiation and X'Celerator multi-strip detector. Each measurement was made within an angular range of  $2\theta = 5$ -50° and lasted overnight. The  $\text{Cu-K}\alpha_1$  radiation was generated at 45 KV and 40 mA ( $\lambda = 1.5059$  Å).

The samples were put on sample holders made of Si wafer to reduce background and flattened with a razor blade.

**DSC measurements.** DSC experiments were performed on Perkin Elmer DSC8000 coupled with CLN2 for thermalisation of the calorimetric bloc. The samples were introduced in standard aluminium sample pan and put inside the calorimeter. We took particular care considering sample shaping and thermal transfer for both ceramic and powder by using similar mass (ca. 15-20 mg) and thickness of samples in order to insure the best comparability of results.

Cycles were performed at different rate from 0.5 K min<sup>-1</sup> to 30 K min<sup>-1</sup> under an argon flux of 40 ml min<sup>-1</sup>.



**Magnetic measurements.** Magnetic measurements were performed using a vibrating sample magnetometer (VSM MicroSense EZ7) operating at 15 kOe of applied magnetic field. The weighted powder samples ( $\approx 5 - 10$  mg) were sealed into a tin capsule then glued onto a quartz fibre and placed in a nitrogen flux furnace between the magnets. The diamagnetic contribution of the quartz and the tin were subtracted from the data using a blank experiment. The procedure consisted to cycle the samples between 300 K and 420 K twenty times for each of them. The thermal cycles were performed at 5 K min<sup>-1</sup> scan rate for all the measurements.

**Diametral compression test.** Diametral compression tests were performed using a TA.HDplus texture analyser (Stable microsystems, United Kingdom). Compacts were compressed between two flat surfaces at a constant speed of 0.10 mm/s with an acquisition rate of 500 Hz. The breaking force  $F_r$  of each tablet was recorded. The maximum tensile strength  $\sigma_T$  of each tablet was evaluated using the equation:

$$\sigma_T = \frac{2F}{\pi Dh}$$

where  $h$  and  $D$  are respectively the tablet height and diameter.

## Result and discussion

**Starting material characterization.** The SCO complex  $[\text{Fe}(\text{Htrz})_2(\text{trz})]\cdot\text{BF}_4$  (**1**) was synthesized following the previously described procedure by addition under continuous stirring at 80 °C of an ethanolic solution of Htrz into a aqueous solution of  $\text{Fe}(\text{BF}_4)_2$ .<sup>61</sup> After drying, the resulting pink powder corresponds to the desired compound (Elem. Anal. Calcd for  $\text{C}_6\text{H}_8\text{N}_3\text{FeBF}_4$  wt%: C: 20.6; H: 2.3; N: 36.1; B: 3.1; Fe: 16.0. Found: C: 20.1; H: 2.3; N: 34.5; B: 3.4, Fe: 14.6). X-ray powder diffraction pattern of **1** reveals a well crystallized compound corresponding to the previously described polymorph I made of interacting  $[\text{Fe}(\text{Htrz})_2(\text{trz})]^+$  chains where Htrz and trz- act as bridging ligands.<sup>62,63</sup> Rietveld refinement of **1** has been performed using JANA2006<sup>64</sup> and Fullprof softwares<sup>65</sup> using the previously described crystal structure as a starting point.<sup>62</sup> The calculated profile fits very well the experimental pattern ( $R_{\text{wp}} = 0.10$ ,  $R_p = 0.07$ ,  $R_{\text{bragg}} = 0.07$ ), what confirms the crystal structure of **1** (figure 1). After subtraction of instrumental broadening, sample contribution to peak broadening could be estimated to a mean coherent domain size of ca. 50 nm and micro-deformations of ca.  $20 \cdot 10^{-4}$ . Furthermore, the coherent domain sizes are anisotropic with a strong elongation along the  $b$  parameter corresponding to the chain direction (260 nm in the  $b$  direction and 34 nm in the  $ac$  directions). These observations are in line with the particles size observed by TEM (figure S1) and with the previously reported results on the same compound<sup>66</sup> except that coherent domains size are smaller in our case, probably due to the synthetic procedure.

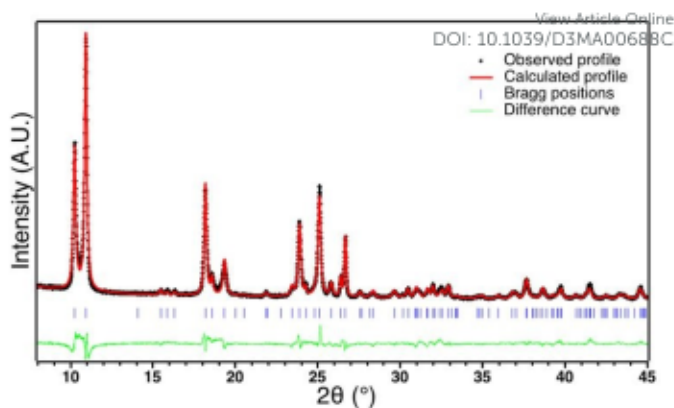


**Figure 1.** Rietveld refinement results on powder X-ray diffraction pattern of **1** at 293 K. Experimental pattern (black cross), calculated pattern using polymorph I data (red line), Difference curve (green line), Bragg positions (vertical lines)

**Magnetic behaviour of the starting powder.** Magnetic properties of **1** were recorded on a Vibrating Sample Magnetometer (VSM). At 300 K the  $\chi_M T$  product (where  $\chi_M$  is the molar magnetic susceptibility and  $T$  the temperature) is around  $0.3 \text{ cm}^3 \text{ K}^{-1} \text{ mol}^{-1}$  corresponding to a  $\text{Fe}^{2+}$  in the Low Spin (LS) state with a slight High Spin (HS) residual fraction. On warming,  $\chi_M T$  product remains close to 0 up to 380 K and increases abruptly above 380 K to reach a value of  $3.5 \text{ cm}^3 \text{ K}^{-1} \text{ mol}^{-1}$  at 400 K as expected for a  $\text{Fe}^{2+}$  ion in the HS state. This value remains stable till 420 K. On cooling, the  $\chi_M T$  product remains around the fully HS value before rapidly falling down to ca.  $0.3 \text{ cm}^3 \text{ K}^{-1} \text{ mol}^{-1}$  at 340 K, signature of an almost complete HS to LS conversion (figure 2). It remains close to  $0.3 \text{ cm}^3 \text{ K}^{-1} \text{ mol}^{-1}$  on cooling to 250 K. These features are characteristic of a cooperative SCO with a 40K wide hysteresis ( $T_{1/2\uparrow} = 380 \text{ K}$  and  $T_{1/2\downarrow} = 340 \text{ K}$ ) as expected for the polymorph I of this compound. Several cycles (one cycle corresponding to crossovers from LS to HS in warming mode followed by HS to LS in cooling mode) were then performed between 300 and 420 K to evaluate the evolution of the hysteresis loop upon cycling. The first ten cycles showed a strong modification of the transition temperatures that decrease by almost 10 K in the warming mode ( $T_{1/2\uparrow}$ ) leading to a smaller hysteresis loop. The next ten cycles showed a smaller evolution of both  $T_{1/2\downarrow}$  and  $T_{1/2\uparrow}$ . It is worth to note that a tens of cycles are thus required to reach a “stabilized” hysteresis loop for which  $T_{1/2\downarrow}$  and  $T_{1/2\uparrow}$  converge to 341K and 374K respectively leading to a 33 K stable hysteresis loop for this compound (figure S2a). Therefore, upon thermal cycling, the width of the hysteresis decreases as a reflect of a weakening of the cooperative character of the compound. This might correspond to a fatigability of the sample, as already reported.<sup>66</sup> It is also important to mention that cooperativity is related to either the abruptness of the switching (the temperature range of the LS  $\leftrightarrow$  HS switching) or the width of the thermal hysteresis. Several thermodynamic models were developed to account for both characteristics and will be discussed in the following sections.





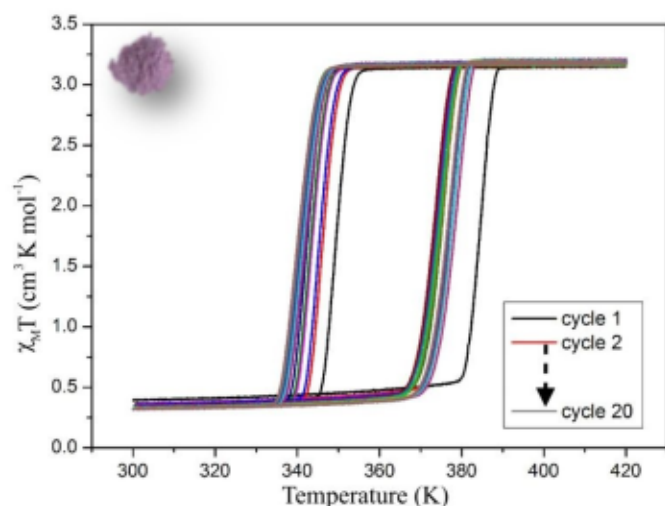


**Figure 2.**  $\chi_m T$  product versus  $T$  recorded on a powder sample of **1** showing the evolution of the magnetic properties upon 20 cycles. Scan rate = 5 K min<sup>-1</sup>.

**DSC measurements on the starting powder.** The deviation from normal heat capacity ( $\Delta C_p$ ) has been recorded upon twenty cycles and is reported for the starting powder sample on figure 3. Two peaks corresponding to the LS  $\rightarrow$  HS, and HS  $\rightarrow$  LS SCO in the warming and cooling modes, respectively, are clearly detected. As already observed with magnetic measurements, a strong evolution of the two  $T_{1/2}$  is observed upon cycling, which is more pronounced concerning  $T_{1/2\downarrow}$ . It is worth to note that at least 10 cycles are needed before reaching a stabilized hysteresis loop with  $T_{1/2\uparrow}$  and  $T_{1/2\downarrow} = 374$  K and 343 K respectively, perfectly matching the magnetic behaviour (figure 2 and S2a). Additionally, a significant decrease of the absolute value peak maxima or minima accompanied by an enlargement of the peak is clearly visible on figure 3. The LS  $\leftrightarrow$  HS switching thus takes place on a wider temperature range upon cycles on either ascending or descending branches indicating a decrease of the abruptness of this switching. This effect may be linked to

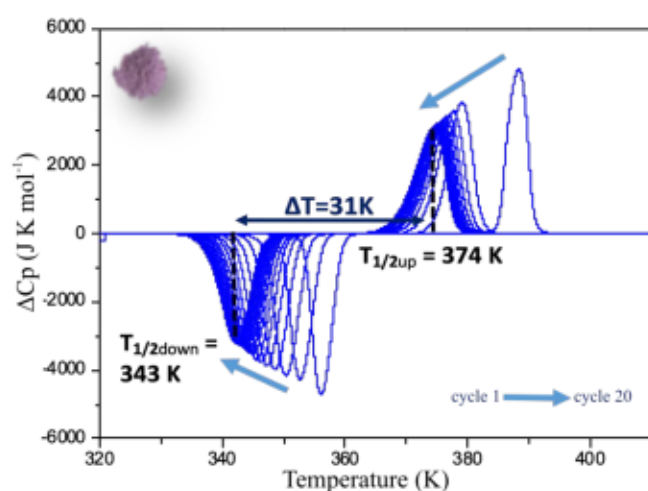


**Figure 3.** Deviation from normal molar heat capacity ( $\Delta C_p$ ) vs temperature for **1** recorded by DSC on a powder sample at 5 K min<sup>-1</sup>. Arrows are showing the evolution from the first to the 20<sup>th</sup> cycle.  $\Delta C_p$  peaks in the cooling mode are artificially represented negatives, that way, endothermic process correspond to a positive peak in the chart.

the structural fatigability that is evidenced by the decrease of the coherent domain sizes and the slight modification of the cell parameters after cycling (figure S3). Two effects, thus, go with the thermal cycling: a lowering of the transition temperatures and a decrease of the cooperativity of the LS  $\rightarrow$  HS, and HS  $\rightarrow$  LS SCO as shown by the increase of DSC peak widths.

**Elaboration of ceramics.** Even if this compound is not purely molecular due to its 1-D polymeric nature, ceramics of **1** fall into the definition of "molecular ceramics" given in reference 10. Such molecular ceramics of **1**, were then prepared by Cool-SPS. Different sintering parameters and sequences were explored and optimized (pressure, temperature, ramps...), to design an efficient Cool-SPS process. Sintering sequences for which the temperature was applied before pressure were found adequate and extensively explored with respect to Cool-SPS accessible conditions ( $50 \leq T \leq 600^\circ\text{C}$ ,  $40 \leq P \leq 600$  MPa). The sintering map obtained (see figure S4) revealed that combining high temperatures and pressures ( $T \geq 300^\circ\text{C}$ ,  $P > 400$  MPa) is detrimental to the stability of **1**, while operating at either low temperature ( $T \leq 200^\circ\text{C}$ ) or pressure ( $P < 200$  MPa) would not yield dense ceramics. The highest densifications (95% of relative density, where the relative density is the ratio between the geometrically measured density of the pellets and the density of the corresponding single crystal) were obtained for temperatures ranging between 250 and 300  $^\circ\text{C}$ , and pressures between 300 and 400 MPa.

**Mechanical testing of molecular ceramics.** Application of a significant pressure during a low temperature sintering process always question the nature of the obtained samples, which may be dense but poorly cohesive compacts lacking intergranular bonding, or ceramics showing improved strength thanks to optimized intergranular bonding through sintering. To address this point, a series of twelve ceramics (3 ceramics per processing conditions from which nine could be used in diametral compression test) was specifically elaborated and brought under a breaking test to evaluate their cohesiveness. Except for samples of lowest density, ceramics obtained by Cool-SPS typically required a larger tensile strength to reach a given displacement, demonstrating their higher cohesiveness, as compared to cold pressed powders (see figure S5a) of similar relative density. This trend is confirmed when differentiating the elastic part of the mechanical response (see figure S5b), where Cool-SPS ceramics display slopes ranging from 26 to 42 MPa/mm, versus 24 to 27 MPa/mm for cold-pressed samples, *i.e.* an increase of almost 50% in the best case. Since all samples are constituted of the same compound, displaying the same crystal structure, these results confirm a significant level of intergranular bonding in Cool-SPS processed molecular ceramics, responsible for their increased strength. Thus, providing they kept their SCO behaviour, the most cohesive and dense samples potentially form the first series of functional molecular ceramics. To establish this point, a ceramic of **1** of 95 % relative density denoted from now **C1** underwent a complete set of characterizations identical to those performed on powder (in order i) to check if the functional feature (SCO) was conserved



and ii) to compare the behaviour of the ceramics versus the powders.

**X-Ray diffraction of the ceramics.** X-ray diffraction pattern performed on **C1** is shown on Figure 4. It is clearly very similar to the pattern of the corresponding powder. The Rietveld refinement confirms that the polymorph (I) is preserved after sintering ( $R_{wp} = 0.09$ ,  $R_p = 0.07$ ,  $R_{bragg} = 0.05$ ). Nevertheless some slight structural and/or microstructural details differ. The calculated profile reveals a different shape of coherent domain size and a slightly smaller  $a$  parameter. Even if the mean coherent domain size is of the same order (but slightly smaller: 35 nm), the anisotropic shapes differ: while the apparent sizes in  $a$  and  $c$  directions remain similar to the powder (30 nm vs 34 nm for the powder), the size in the  $b$  direction is significantly smaller (140 nm vs 260 for the powder). Such an effect of the reduction of the coherent domain size has been previously observed on powder after more than 10 cycles and attributed to fatigability<sup>66</sup>, what was also confirmed for powder in this study (figure S3). It was suggested that this microstructural fatigability was accompanied by a subtle structural variation corresponding of a slight rotation of the chain linked to the decrease of the  $a$  parameter.<sup>67</sup> Since a similar evolution of the  $a$  parameter is also detected on ceramics in addition to the reduction of the coherent domain size within the  $b$  direction, it seems then that the sintering process leads to a very similar microstructural and structural evolution, but without cycling.

**Magnetism and DSC of ceramics.** Magnetic properties were recorded on a Vibrating Sample Magnetometer (VSM). Several cycles of warming and cooling were performed on **C1** (Figure 5). For the first cycle, upon warming from 300 K the  $\chi_M T$  product remains around  $0.3 \text{ cm}^3 \text{ K}^{-1} \text{ mol}^{-1}$  till ca. 370 K and increases sharply to reach ca.  $3.25 \text{ cm}^3 \text{ K}^{-1} \text{ mol}^{-1}$  at 380 K and higher, what is a signature of an almost complete LS to HS transition. On cooling the  $\chi_M T$  product remains stable till ca. 345 K and then rapidly decreases to reach  $0.3 \text{ cm}^3 \text{ K}^{-1} \text{ mol}^{-1}$ , corresponding to the HS to LS SCO with a small amount of remaining HS

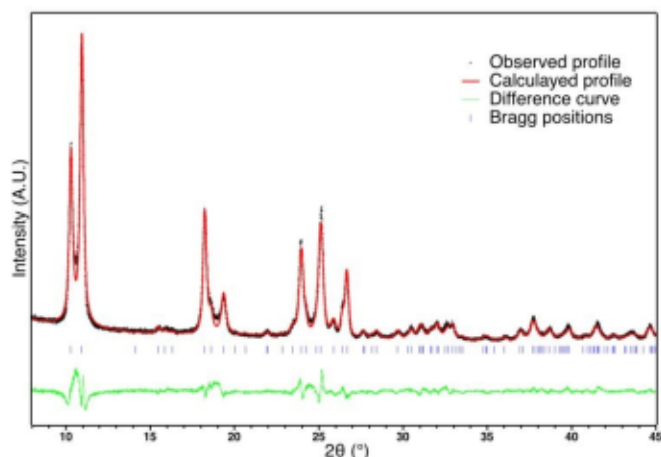


**Figure 4.** Rietveld refinement results on powder X-ray diffraction pattern of molecular ceramic of **1** at 293 K. Experimental pattern (black cross), calculated pattern (red line), Difference curve (green line), Bragg positions (vertical lines).

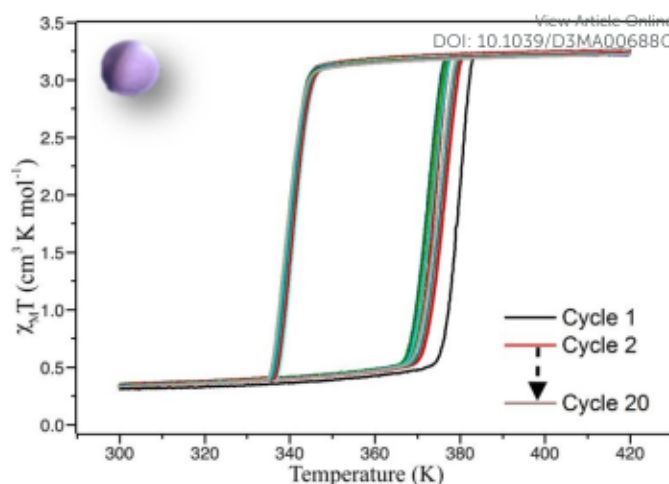


**Figure 5.**  $\chi_M T$  product versus  $T$  recorded on a molecular ceramic of **1** showing the evolution of the magnetic properties upon 20 cycles. Scan rate =  $5 \text{ K min}^{-1}$ .

complexes below the transition temperature. This feature proves that after sintering the molecular ceramics has conserved its SCO functionality, corresponding to a cooperative spin transition with a 39 K hysteresis width ( $T_{1/2\uparrow} = 379 \text{ K}$  and  $T_{1/2\downarrow} = 340 \text{ K}$ ). Upon cycling between 300 and 400 K an evolution of the transition temperatures is clearly observed. Interestingly, this phenomenon is much less pronounced than for the powder especially in the cooling mode.  $T_{1/2\uparrow}$  decreases to 374 K whereas  $T_{1/2\downarrow}$  remains almost unchanged around 340 K, leading to a hysteresis loop of 34 K wide equivalent to the powder behaviour after 20 cycles (Figure S2b). The stabilized hysteresis loops of powder and ceramic are thus very similar even if the ceramic seems to present a slightly more abrupt transition ( $\Delta T_{60} = 6.1 \text{ K}$  for ceramic, vs 7.4 K for powder in warming mode, where  $\Delta T_{60}$  is the temperature range in which 60 % of the iron ions (from 80 % LS to 80 % HS) undergo the SCO.<sup>68</sup>

As for the powder, a full DSC study has been performed on **C1** following the same procedure. The deviation from the normal heat capacity ( $\Delta C_p$ ) has been recorded upon twenty cycles and the two peaks corresponding to the LS  $\rightarrow$  HS, and HS  $\rightarrow$  LS transitions in the warming and cooling mode respectively are shown upon the different cycles on figure 6. The evolution of the positions of the peaks differs significantly from that observed for the powder. Although in this case, conversely to magnetic behaviour, a very singular first cycle is observed, the subsequent cycles behave differently. Indeed,  $T_{1/2\uparrow}$ , as for powder, slightly decreases to reach 374 K, but  $T_{1/2\downarrow}$  increases instead, to stabilize much more rapidly than for the powder after few cycles at 343 K. This behaviour is in line with the magnetic measurements confirming that the ceramic is already close to the stabilized state after sintering. This can be related to X-ray diffraction results that showed that the structural and microstructural properties after sintering are closer to those observed after several cycles on the powder. Sintering process



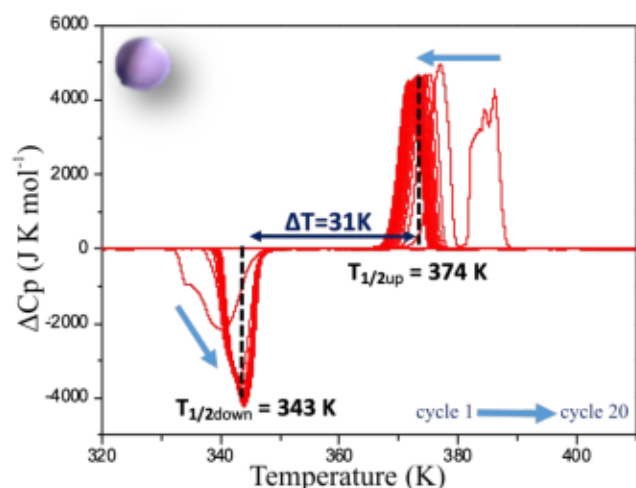


**Figure 6.** Deviation from normal molar heat capacity ( $\Delta C_p$ ) vs temperature for a molecular ceramic of **1** recorded by DSC at  $5 \text{ K min}^{-1}$ . Arrows are showing the evolution from the first to the 20<sup>th</sup> cycle.

would thus induce structural and microstructural modifications in the polycrystalline sample. As a consequence, only 5 cycles are needed to get a stabilized hysteresis loop from the molecular ceramics, versus 12 for the powder (Figure S6). It is worth to note that, conversely to the powder, the absolute value of the DSC peak maxima or minima do not change, leading to the same peak widths and heights upon cycling. Thus, cycling the ceramics do not modify the abruptness/cooperativity of the transition demonstrating a limited fatigability. Additionally, comparing the absolute values of DSC peak maxima or minima for the ceramic and the powder show that they are systematically higher in the molecular ceramics with respect to the powder, what correspond to narrower peaks and then more steep transitions.

**Discussion.** Powder of the SCO material  $[\text{Fe}(\text{Htrz})_2(\text{trz})]\text{BF}_4$  has been successfully used to produce molecular ceramics with relative density as high as 95%. Either from magnetic or DSC measurements, the conservation of the SCO property in the molecular ceramics is undisputable, with the same global behaviour than the starting powder. X-ray diffraction study shown that Cool-SPS processing did not induce any irreversible phase transition as the structural analysis confirmed that the ceramics correspond to the same polymorph than the starting powder (recognized as polymorph I<sup>63</sup>). Nevertheless, the Rietveld refinement revealed that the sintering process induced structural and microstructural changes similar to those observed upon cycling with the powder.<sup>66,69</sup> It is worth mentioning that one cycle of LS-HS-LS transition is occurring during SPS process due to pressure/temperature modification, which can be partially detected onto SPS monitoring (figure S7). This structural and microstructural relaxations lead to quicker stabilization of the hysteresis loop upon cycling for the ceramic as compared to the powder, what is well illustrated by the magnetic behaviour of both sample and even more clearly revealed by DSC. The main difference remaining after cycling between powder and ceramic concerns the sharpness of the transition that is significantly more pronounced for ceramics

than for powder according to DSC results. To go further on that point, DSC measurements have been used to obtain the thermodynamic features of both samples and implemented in well-known thermodynamic models such as the Slitcher & Drickamer (S&D)<sup>70</sup> or Sorai & Seki (S&S)<sup>71</sup> ones. In order to emphasize only the differences between stabilized SCO behaviours, it is mandatory to work on cycles greater than the 10<sup>th</sup> one, we chose then to work on the 12<sup>th</sup> cycle. Integration of the  $\Delta C_p$  peaks and  $\Delta C_p/T$  peaks over  $T$  gave respectively the variation of enthalpy and entropy of the samples at the SCO. Results are gathered in Table 1. The obtained values for the variation of enthalpy at the transition in the warming and cooling modes  $\Delta H_{\uparrow}$  and  $\Delta H_{\downarrow}$  are very similar, demonstrating that the transition is fully reversible for both samples (powder and ceramic). Then, the mean value has been chosen for  $\Delta H$  in both cases. Conversely, as this compound is associated with an hysteretic behaviour, two distinct values of  $\Delta S$  corresponding to  $T_{1/2\uparrow}$  and  $T_{1/2\downarrow}$  are obtained, the real one (used in the S&D model) should lie in between these two values but is not necessary the average. The thermodynamic values obtained that way are very similar for powder and molecular ceramic and close to those found in the literature for this compound.<sup>72</sup> It confirms that the SCO phase transition involves the same polymorph (polymorph I) in both cases. Nevertheless, variation of enthalpy of ceramic is slightly lower than powder probably due to a somewhat less complete transition for the ceramic as suggested by the slightly lower  $\chi_{\text{MT}}$  product obtained for the ceramic above 380K.

These thermodynamic parameters have been then introduced into the S&D model to evaluate the so-called cooperativity parameter  $\Gamma$ . The fit of the magnetic curves that is illustrated by figure S8 leads to the same value of  $\Gamma$  for both samples (table 1). It is not surprising since i) the stabilized SCO cycles correspond to the same hysteresis width and ii)  $\Gamma$  is representative of intermolecular interactions that should be the same between powder and ceramics as both correspond to the same polymorph. Because the S&D model cannot explain the difference in abruptness between both samples we also used the S&S model which introduces the notion of cooperative domains. This model uses the number  $n$  that represent the number of metal centres undergoing the SCO simultaneously. Thus, the higher the  $n$  number and the more cooperative the transition, the more abrupt SCO. Since this model cannot account for hysteretic behaviours, we used only the LS to HS transition and fit the corresponding DSC peak with the S&S model to extract  $n$ . Figure S9 shows the result of the fit for both samples on the 12<sup>th</sup> cycle leading to  $n_p = 17$  for the powder and

**Table 1.** Thermodynamic parameters extracted from DSC measurements and S&D model.

Sample	$\langle \Delta H \rangle$ kJ mol <sup>-1</sup>	$\Delta S_{\uparrow}$	$\Delta S_{\downarrow}$	$\Delta S$ (S&D)	$\Gamma$ J mol <sup>-1</sup>
Powder	26.3	68.6	77.7	73.2	8500
Ceramic	24.9	65.2	73.3	69.3	8500





## ARTICLE

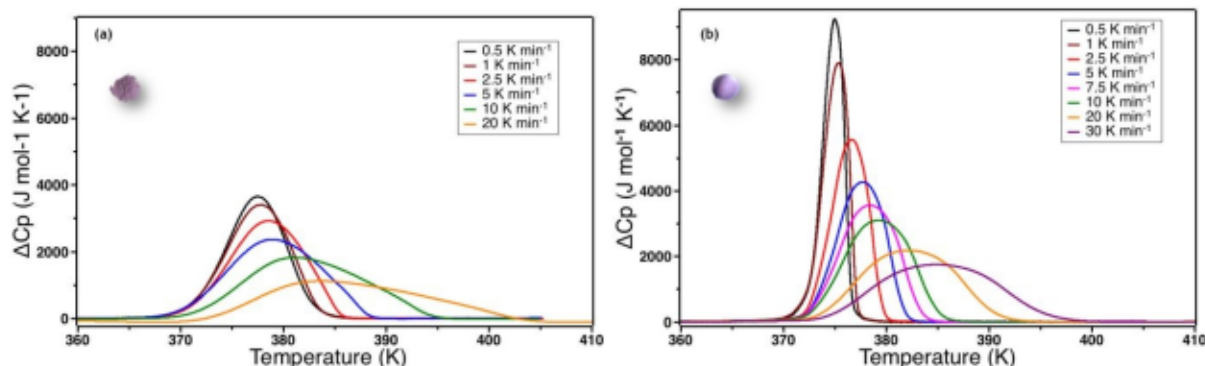


Figure 7. Scan rate effect on the  $\Delta C_p$  peaks for (a) powder and (b) molecular ceramics of 1.

$n_c = 35$  for the ceramic. This agrees with a steeper and more cooperative transition observed in ceramics.

In order to check how this parameter depends on thermal conduction capability of the samples, we also explore the effect of the temperature scan rate. Figure 7 shows the  $\Delta C_p$  over  $T$  curves for different scan rates for powder and ceramic between  $0.5 \text{ K min}^{-1}$  to  $30 \text{ K min}^{-1}$ .

Three observations can be done: i) at  $1 \text{ K min}^{-1}$ , the scan rate is high enough to artificially increase the width of the transition; ii) the  $\Delta C_{p_{\max}}$  values are systematically higher for the ceramic than for the powder even at very low scan rates and iii)  $\Delta C_p$  peak widths and maxima did not converge between ceramics and powders even at very low scan rates. As  $\Delta C_{p_{\max}}$  directly influences the value of  $n$  in the S&S model, the value of  $n$  tends to artificially decrease when the scan rate increases. Nevertheless, as  $\Delta C_{p_{\max}}$  are systematically higher for the

ceramic than for the powder, the value of the  $n$  S&S parameter may be effectively higher for the ceramics. In order to overcome this scan rate effect we calculated the  $n$  parameter by fitting the DSC peaks of the powder ( $n_p$ ) and ceramic ( $n_c$ ) for all scan rates using the S&S model. The results are presented in the Figure 8 and show that  $n_c$  is indeed systematically higher than  $n_p$  at any scan rate and the effect is hindered at high rates. By extrapolating this evolution of  $n$  to scan rate =  $0 \text{ K min}^{-1}$ , one can evaluate the limit of the  $n$  value for the powder and the ceramic, ridding off the scan rate effect. The limit cooperative domain sizes are found, that way, to be  $n_p = 26$  and  $n_c = 84$  for the powder and the ceramic, respectively. The sintering of the powder into a molecular ceramic tends thus to increase the cooperative domains size, that becomes triple that of the corresponding powder. When scan rate is increasing, the cooperative domains size rapidly decreases for ceramics, while it is much less affected for powder, what can be due to a better thermal conductivity of ceramics.

Thereby, while grinding process was proven to affect the SCO by decreasing the cooperativity directly linked to smaller crystal coherent domain sizes, sintering by Cool-SPS, even if the influence is smaller, leads to the opposite effect probably due to improvement of thermal conductivity of the sintered samples. It could be then an interesting tool for the understanding the possible different kind of cooperativity in SCO compounds for example: microscopic intrinsic cooperativity and macroscopic microstructurally dependent cooperativity.

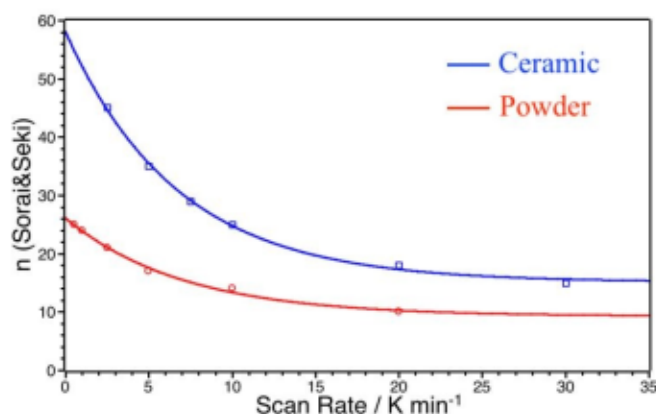


Figure 8. Evolution of the cooperative domain size parameter  $n$  obtain from the S&S model for different temperature scan rates for powder (red circles) and ceramic (blue squares).



## Conclusion.

Shaping of SCO materials has been widely studied during the last decade, from thick to thin film, bulk to nanomaterials, composites or alloys but the molecular ceramic form has not been investigated so far. Thanks to Cool-SPS, we have demonstrated that high density and cohesive functional molecular ceramics are accessible. Starting from the model  $[\text{Fe}(\text{trz})_2(\text{Htrz})]\text{BF}_4$  SCO cooperative compound, we have obtained a new molecular ceramic of 95% relative density with the complete conservation of the SCO functionality. The global behaviour (transition temperature, hysteresis width) was preserved. This new way of shaping the SCO compounds is thus very promising for the insertion of SCO materials into specific devices using traditional ceramics, but also enables a more easy and reliable access to some specific measurements like dielectric, polarization or conductivity properties as well as to the conception of composites.

Additionally, on an academic point of view, the deep investigation using simple thermodynamic models showed that SCO molecular ceramics presents larger "cooperative domains" than the corresponding powders. Sintering would then improve the interdomain pathways to increase cooperativity at the macroscopic level probably due to much better thermal conduction capabilities. These specificities offer the opportunities to better understand both the notion of cooperativity in SCO materials and the notion of molecular ceramic itself, in which, beyond the contribution of intermolecular forces to cohesiveness at the coherent domains scale, functional properties like SCO are expressed beyond the boundaries of single particles or coherent domains.

## Author Contributions

The manuscript was written through contributions of all authors. All authors have given approval to the final version of the manuscript.

**MM** wrote the manuscript and supervised all the work, **LEK** performed the synthesis of all samples and supervised the characterizations, **ND** synthesized the starting powder, **MJ** made and supervised the sintering of the samples, **DD** and **LE** performed the DSC analysis, **PR** supervised the magnetic measurements and chemical analysis **CG** checked the thermodynamic models and carefully read over the whole manuscript, **VM** performed the diametral compression of pellets.

## Conflicts of interest

The authors declare no conflict of interest.

## Acknowledgment

This work was supported by the ANR-19-CE07-0026 (MEMORI). We acknowledge Centre National de la Recherche Scientifique (CNRS), University of Bordeaux and Bordeaux INP for technical support and Lebanon state for part of PhD. grant of Liza El-

Khoury. Michaël Josse thanks CNRS and University of Bordeaux for 6 months sabbatical leaves during 2017-2018 and 2019-2020, for the development of molecular ceramics and Cool-SPS. The X-ray diffraction facility of the ICMCB is thanked for the powder diffraction experiments and more particularly Eric Lebraud for his useful technical support. We thank also U-Chan Chung for his support for the SPS. The UAR 3626 PLACAMAT is acknowledged for the TEM facilities and more specifically Marion Gayot for her help.

## Notes and references

- 1 G. Barreto, P. Canhoto and M. Collares-Pereira, Parametric analysis and optimisation of porous volumetric solar receivers made of open-cell SiC ceramic foam, *Energy*, 2020, **200**, 117476.
- 2 X. Kong, L. Yang, Z. Cheng and S. Zhang, Bi-modified  $\text{SrTiO}_3$ -based ceramics for high-temperature energy storage applications, *J. Am. Ceram. Soc.*, 2020, **103**, 1722–1731.
- 3 E. A. Mikhaleva, I. N. Flerov, E. V. Bogdanov, V. S. Bondarev, M. V. Gorev and E. Rysiakiewicz-Pasek, Size effect on sensitivity to external pressure and caloric effects in TGS: Ceramics and nanocomposites, *Mater. Today Commun.*, 2020, **25**, 101463.
- 4 K. Zou, Y. Dan, H. Xu, Q. Zhang, Y. Lu, H. Huang and Y. He, Recent advances in lead-free dielectric materials for energy storage, *Mater. Res. Bull.*, 2019, **113**, 190–201.
- 5 J. Guo, R. Floyd, S. Lowum, J.-P. Maria, T. Herisson de Beauvoir, J.-H. Seo and C. A. Randall, Cold Sintering: Progress, Challenges, and Future Opportunities, *Annu. Rev. Mater. Res.*, 2019, **49**, 275–295.
- 6 J.-P. Maria, X. Kang, R. D. Floyd, E. C. Dickey, H. Guo, J. Guo, A. Baker, S. Funihashi and C. A. Randall, Cold sintering: Current status and prospects, *J. Mater. Res.*, 2017, **32**, 3205–3218.
- 7 M. T. Sebastian, H. Wang and H. Jantunen, Low temperature co-fired ceramics with ultra-low sintering temperature: A review, *Curr. Opin. Solid State Mater. Sci.*, 2016, **20**, 151–170.
- 8 S. Li, X. Wang, J. Ren, C. Liu, Y. Hu and Y. Yang, Microstructure, mechanical property and corrosion behavior of biomedical Zn-Fe alloy prepared by low-temperature sintering, *J. Alloys Compd.*, 2023, **934**, 167812.
- 9 T. Herisson de Beauvoir, A. Sangregorio, A. Bertrand, C. Payen, D. Michau, U.-C. Chung and M. Josse, Cool-SPS stabilization and sintering of thermally fragile, potentially magnetoelectric,  $\text{NH}_4\text{FeP}_2\text{O}_7$ , *Ceram. Int.*, 2019, **45**, 9674–9678.
- 10 T. Herisson de Beauvoir, V. Villemot and M. Josse, Cool-Spark plasma sintering: An opportunity for the development of molecular ceramics, *Solid State Sci.*, 2020, **102**, 106171.
- 11 T. Herisson de Beauvoir, A. Sangregorio, I. Cornu, C. Elissalde and M. Josse, Cool-SPS: an opportunity for low temperature sintering of thermodynamically fragile materials, *J. Mater. Chem. C*, 2018, **6**, 2229–2233.





- 12 E. Coronado, Molecular magnetism: from chemical design to spin control in molecules, materials and devices, *Nat. Rev. Mater.*, 2020, **5**, 87–104.
- 13 B. L. Feringa and W. R. Browne, *Molecular Switches*, Wiley-VCH Verlag GmbH & Co. KGaA, Weinheim, Germany, 2011, vol. 1.
- 14 M. D. Manrique-Juárez, S. Rat, L. Salmon, G. Molnár, C. M. Quintero, L. Nicu, H. J. Shepherd and A. Bousseksou, Switchable molecule-based materials for micro- and nanoscale actuating applications: Achievements and prospects, *Coord. Chem. Rev.*, 2015, **308**, 395–408.
- 15 Y.-S. Meng, O. Sato and T. Liu, Manipulating Metal-to-Metal Charge Transfer for Materials with Switchable Functionality, *Angew. Chemie Int. Ed.*, 2018, **57**, 12216–12226.
- 16 J.-P. Sauvage, V. Amendola, R. Ballardini, V. Balzani, A. Credi, L. Fabbrizzi, M. T. Gandolfi, J. K. Gimzewski, M. Gómez-Kaifer, C. Joachim, A. E. Kaifer, E. Katz, T. R. Kelly, J. Liu, C. Mangano, P. Pallavicini, A. R. Pease, L. Raehm, M. Sano, J.-P. Sauvage, J. P. Sestelo, A. N. Shipway, J.-F. Stoddart, M. Venturi and I. Willner, Eds., *Molecular Machines and Motors*, Springer Berlin Heidelberg, Berlin, Heidelberg, 2001, vol. 99.
- 17 M. A. Halcrow, *Spin-Crossover Materials*, John Wiley & Sons Ltd, Oxford, UK, 2013.
- 18 H. Li and H. Peng, Recent advances in self-assembly of spin crossover materials and their applications, *Curr. Opin. Colloid Interface Sci.*, 2018, **35**, 9–16.
- 19 G. Molnár, S. Rat, L. Salmon, W. Nicolazzi and A. Bousseksou, Spin Crossover Nanomaterials: From Fundamental Concepts to Devices, *Adv. Mater.*, 2018, **30**, 1703862.
- 20 K. Ridier, A.-C. Bas, Y. Zhang, L. Routaboul, L. Salmon, G. Molnár, C. Bergaud and A. Bousseksou, Unprecedented switching endurance affords for high-resolution surface temperature mapping using a spin-crossover film, *Nat. Commun.*, 2020, **11**, 3611.
- 21 K. S. Kumar and M. Ruben, Sublimable Spin-Crossover Complexes: From Spin-State Switching to Molecular Devices, *Angew. Chemie Int. Ed.*, 2021, **60**, 7502–7521.
- 22 K. Senthil Kumar and M. Ruben, Emerging trends in spin crossover (SCO) based functional materials and devices, *Coord. Chem. Rev.*, 2017, **346**, 176–205.
- 23 X. Zhang, T. Palamarciuc, J.-F. Létard, P. Rosa, E. V. Lozada, F. Torres, L. G. Rosa, B. Doudin and P. A. Dowben, The spin state of a molecular adsorbate driven by the ferroelectric substrate polarization, *Chem. Commun.*, 2014, **50**, 2255.
- 24 A. Bousseksou, N. Negre, M. Goiran, L. Salmon, J. P. Tuchagues, M. L. Boillot, K. Boukheddaden and F. Varret, Dynamic triggering of a spin-transition by a pulsed magnetic field, *Eur. Phys. J. B*, 2000, **13**, 451–456.
- 25 G. Chastanet, M. Lorenc, R. Bertoni and C. Desplanches, Light-induced spin crossover—Solution and solid-state processes, *Comptes Rendus Chim.*, 2018, **21**, 1075–1094.
- 26 S. Decurtins, P. Gülich, C. P. Köhler, H. Spiering and A. Hauser, Light-induced excited spin state trapping in a transition-metal complex: The hexa-1-propyltetrazole-iron (II) tetrafluoroborate spin-crossover system, *Chem. Phys. Lett.*, 1984, **105**, 1–4. DOI: 10.1039/D3MA00688C
- 27 C. Lefter, R. Tan, J. Dugay, S. Tricard, G. Molnár, L. Salmon, J. Carrey, W. Nicolazzi, A. Rotaru and A. Bousseksou, Unidirectional electric field-induced spin-state switching in spin crossover based microelectronic devices, *Chem. Phys. Lett.*, 2016, **644**, 138–141.
- 28 Y. Qi, E. W. Müller, H. Spiering and P. Gülich, The effect of a magnetic field on the high-spin  $\rightleftharpoons$  low-spin transition in  $[\text{Fe}(\text{phen})_2(\text{NCS})_2]$ , *Chem. Phys. Lett.*, 1983, **101**, 503–505.
- 29 M. Enamullah and W. Linert, Spin-crossover of  $[\text{Fe}(\text{Cl-bzimpy})_2](\text{ClO}_4)_2$  induced by deprotonation, *J. Coord. Chem.*, 1995, **35**, 325–335.
- 30 F. Renz, P. A. De Souza, G. Klingelhöfer and H. A. Goodwin, Molecular Sensors for Moisture Detection by Mössbauer Spectroscopy, in *Industrial Applications of the Mössbauer Effect*, Springer Netherlands, Dordrecht, 2002, pp. 699–704.
- 31 E. Resines-Urien, E. Fernandez-Bartolome, A. Martinez-Martinez, A. Gamonal, L. Piñeiro-López and J. S. Costa, Vapochromic effect in switchable molecular-based spin crossover compounds, *Chem. Soc. Rev.*, 2022, **52**, 705–727.
- 32 P. Guionneau, Crystallography and spin-crossover. A view of breathing materials., *Dalt. Trans.*, 2014, **43**, 382–393.
- 33 W. Nicolazzi, Thermodynamical aspects of the spin crossover phenomenon, *Comptes Rendus Chim.*, 2018, **21**, 1060–1074.
- 34 T. Guillon, S. Bonhommeau, J. S. Costa, A. Zwick, J.-F. Létard, P. Demont, G. Molnár and A. Bousseksou, On the dielectric properties of the spin crossover complex  $[\text{Fe}(\text{bpp})_2](\text{BF}_4)_2$ , *Phys. status solidi*, 2006, **203**, 2974–2980.
- 35 C. Lefter, V. Davesne, L. Salmon, G. Molnár, P. Demont, A. Rotaru and A. Bousseksou, Charge Transport and Electrical Properties of Spin Crossover Materials: Towards Nanoelectronic and Spintronic Devices, *Magnetochemistry*, 2016, **2**, 18.
- 36 C. Lefter, I. A. Gural'skiy, H. Peng, G. Molnár, L. Salmon, A. Rotaru, A. Bousseksou and P. Demont, Dielectric and charge transport properties of the spin crossover complex  $[\text{Fe}(\text{Htrz})_2(\text{trz})](\text{BF}_4)$ , *Phys. status solidi – Rapid Res. Lett.*, 2014, **8**, 191–193.
- 37 P. Guionneau, M. Marchivie, G. Bravic, J.-F. Létard and D. Chasseau, Structural Aspects of Spin Crossover. Example of the  $[\text{Fe}^{\text{II}}\text{L}_n(\text{NCS})_2]$  Complexes, *Top. Curr. Chem.*, 2004, **234**, 97–128.
- 38 M. A. Halcrow, Structure:Function Relationships in Molecular Spin-Crossover Materials, in *Spin-Crossover Materials*, John Wiley & Sons Ltd, Oxford, UK, 2013, pp. 147–169.
- 39 G. Dupouy, M. Marchivie, S. Triki, J. Sala-Pala, J.-Y. Salaün, C. J. Gómez-García and P. Guionneau, The Key Role of the Intermolecular  $\pi$ – $\pi$  Interactions in the Presence of Spin Crossover in Neutral  $[\text{Fe}(\text{abpt})_2\text{A}_2]$  Complexes (A = Terminal Monoanion N Ligand), *Inorg. Chem.*, 2008, **47**, 8921–8931.
- 40 E. Tailleur, M. Marchivie, N. Daro, G. Chastanet and P. Guionneau, Thermal spin-crossover with a large hysteresis spanning room temperature in a mononuclear complex,



- Chem. Commun.*, 2017, **53**, 4763–4766.
- 41 M. G. Reeves, E. Tailleux, P. A. Wood, M. Marchivie, G. Chastanet, P. Guionneau and S. Parsons, Mapping the cooperativity pathways in spin crossover complexes, *Chem. Sci.*, 2021, **12**, 1007–1015.
- 42 T. Delgado and M. Villard, Spin Crossover Nanoparticles, *J. Chem. Educ.*, 2022, **99**, 1026–1035.
- 43 K. S. Kumar and M. Ruben, Sublimable Spin-Crossover Complexes: From Spin-State Switching to Molecular Devices, *Angew. Chemie Int. Ed.*, 2021, **60**, 7502–7521.
- 44 H. J. Shepherd, G. Molnár, W. Nicolazzi, L. Salmon and A. Bousseksou, Spin Crossover at the Nanometre Scale, *Eur. J. Inorg. Chem.*, 2013, **2013**, 653–661.
- 45 L. Kipgen, M. Bernien, F. Tuzek and W. Kuch, Spin-Crossover Molecules on Surfaces: From Isolated Molecules to Ultrathin Films, *Adv. Mater.*, 2021, **33**, 2008141.
- 46 S. Yazdani, J. Phillips, T. K. Ekanayaka, R. Cheng and P. A. Dowben, The Influence of the Substrate on the Functionality of Spin Crossover Molecular Materials, *Molecules*, 2023, **28**, 3735.
- 47 A. Enriquez-Cabrera, A. Rapakousiou, M. Piedrahita Bello, G. Molnár, L. Salmon and A. Bousseksou, Spin crossover polymer composites, polymers and related soft materials, *Coord. Chem. Rev.*, 2020, **419**, 213396.
- 48 P. Guionneau, M. Marchivie and G. Chastanet, Multiscale Approach of Spin Crossover Materials: A Concept Mixing Russian Dolls and Domino Effects, *Chem. – A Eur. J.*, 2021, **27**, 1483–1486.
- 49 M. Romanini, Y. Wang, K. Gürpınar, G. Ornelas, P. Lloveras, Y. Zhang, W. Zheng, M. Barrio, A. Aznar, A. Gràcia-Condal, B. Emre, O. Atakol, C. Popescu, H. Zhang, Y. Long, L. Balicas, J. Lluís Tamarit, A. Planes, M. Shatruk, L. Mañosa, M. Romanini, A. Gràcia-Condal, A. Planes, L. Mañosa, Y. Wang, G. Ornelas, Y. Zhang, M. Shatruk, H. Zhang, Y. Long, K. Gürpınar, O. Atakol, G. G. Ornelas W Brackenridge, P. Lloveras, M. Barrio, A. Aznar, J. L. Tamarit, W. Zheng, L. Balicas and B. Emre, Giant and Reversible Barocaloric Effect in Trinuclear Spin-Crossover Complex  $\text{Fe}_3(\text{bntz})_6(\text{tcnset})_6$ , *Adv. Mater.*, 2021, **33**, 2008076.
- 50 P. Lloveras and J.-L. Tamarit, Advances and obstacles in pressure-driven solid-state cooling: A review of barocaloric materials, *MRS Energy Sustain.*, 2021, **8**, 3–15.
- 51 C. Bartual-Murgui, E. Natividad and O. Roubeau, Critical assessment of the nature and properties of Fe(II) triazole-based spin-crossover nanoparticles, *J. Mater. Chem. C*, 2015, **3**, 7916–7924.
- 52 T. Delgado, C. Enachescu, A. Tissot, A. Hauser, L. Guénée and C. Besnard, Evidencing size-dependent cooperative effects on spin crossover nanoparticles following their HS→LS relaxation, *J. Mater. Chem. C*, 2018, **6**, 12698–12706.
- 53 M. Giménez-Marqués, M. L. García-Sanz De Larrea and E. Coronado, Unravelling the chemical design of spin-crossover nanoparticles based on iron(II)-triazole coordination polymers: Towards a control of the spin transition, *J. Mater. Chem. C*, 2015, **3**, 7946–7953.
- 54 L. Moulet, N. Daro, C. Etrillard, J. F. Létard, A. Grosjean and P. Guionneau, Rational control of spin-crossover particle sizes: From nano-to micro-rods of  $[\text{Fe}(\text{Htrz})_2(\text{trz})](\text{BF}_4)$ , *Magnetochemistry*, 2016, **2**, 10.
- 55 C. Faulmann, J. Chahine, I. Malfant, D. De Caro, B. Cormary and L. Valade, A facile route for the preparation of nanoparticles of the spin-crossover complex  $[\text{Fe}(\text{Htrz})_2(\text{trz})](\text{BF}_4)$  in xerogel transparent composite films, *Dalt. Trans.*, 2011, **40**, 2480–2485.
- 56 A. Suzuki, M. Fujiwara and M. Nishijima, High spin/low spin phase transitions of a spin-crossover complex in the emulsion polymerization of trifluoroethylmethacrylate (TFEMA) using PVA as a protective colloid, *Colloid Polym. Sci.*, 2008, **286**, 525–534.
- 57 A. B. Gaspar, G. Molnár, A. Rotaru and H. J. Shepherd, Pressure effect investigations on spin-crossover coordination compounds, *Comptes Rendus Chim.*, 2018, **21**, 1095–1120.
- 58 J. Linares, E. Codjovi and Y. Garcia, Pressure and temperature spin crossover sensors with optical detection, *Sensors*, 2012, **12**, 4479–4492.
- 59 J. H. Askew, D. M. Pickup, G. O. Lloyd, A. V. Chadwick and H. J. Shepherd, Exploring the Effects of Synthetic and Postsynthetic Grinding on the Properties of the Spin Crossover Material  $[\text{Fe}(\text{atrz})_3](\text{BF}_4)_2$  (atrz = 4-Amino-4H-1,2,4-Triazole), *Magnetochemistry*, 2020, **6**, 44.
- 60 D. Nieto-Castro, F. A. Garcés-Pineda, A. Moneo-Corcuera, B. Pato-Doldan, F. Gispert-Guirado, J. Benet-Buchholz and J. R. Galán-Mascarós, Effect of Mechanochemical Recrystallization on the Thermal Hysteresis of 1D Fe II - triazole Spin Crossover Polymers, *Inorg. Chem.*, 2020, **59**, 7953–7959.
- 61 J. Kroeber, J.-P. Audiere, R. Claude, E. Codjovi, O. Kahn, J. G. Haasnoot, F. Groliere, C. Jay and A. Bousseksou, Spin Transitions and Thermal Hysteresis in the Molecular-Based Materials  $[\text{Fe}(\text{Htrz})_2(\text{trz})](\text{BF}_4)$  and  $[\text{Fe}(\text{Htrz})_3](\text{BF}_4)_2 \cdot \text{H}_2\text{O}$  (Htrz = 1,2,4-4H-triazole; trz = 1,2,4-triazolato), *Chem. Mater.*, 1994, **6**, 1404–1412.
- 62 A. Grosjean, P. Négrier, P. Bordet, C. Etrillard, D. Mondieig, S. Pechev, E. Lebraud, J. Létard and P. Guionneau, Crystal Structures and Spin Crossover in the Polymeric Material  $[\text{Fe}(\text{Htrz})_2(\text{trz})](\text{BF}_4)$  Including Coherent-Domain Size Reduction Effects, *Eur. J. Inorg. Chem.*, 2013, **2013**, 796–802.
- 63 M. Palluel, L. El Khoury, N. Daro, S. Buffière, M. Josse, M. Marchivie and G. Chastanet, Rational direct synthesis of  $[\text{Fe}(\text{Htrz})_2(\text{trz})](\text{BF}_4)$  polymorphs: temperature and concentration effects, *Inorg. Chem. Front.*, 2021, **8**, 3697–3706.
- 64 V. Petříček, M. Dušek and L. Palatinus, Crystallographic Computing System JANA2006: General features, *Zeitschrift für Krist. - Cryst. Mater.*, 2014, **229**, 345–352.
- 65 J. Rodríguez-Carvajal, Recent advances in magnetic structure determination by neutron powder diffraction, *Phys. B Condens. Matter*, 1993, **192**, 55–69.
- 66 A. Grosjean, N. Daro, S. Pechev, L. Moulet, C. Etrillard, G. Chastanet and P. Guionneau, The Spin-Crossover





Phenomenon at the Coherent-Domains Scale in 1D Polymeric Powders: Evidence for Structural Fatigability, *Eur. J. Inorg. Chem.*, 2016, **2016**, 1961–1966.

View Article Online  
DOI: 10.1039/D3MA00688C

- 67 A. Grosjean, Matériaux polymériques 1D à transition de spin : investigations structurales multi-échelles, PhD. thesis, University of Bordeaux, 2013.
- 68 M. Marchivie, P. Guionneau, J.-F. Létard and D. Chasseau, Towards direct correlation between spin crossover and structural properties in iron II complexes, *Acta Crystallogr. B*, 2003, **59**, 479–486.
- 69 A. Grosjean, N. Daro, S. Pechev, C. Etrillard, G. Chastanet and P. Guionneau, Crystallinity and Microstructural Versatility in the Spin-Crossover Polymeric Material [Fe(Htrz)<sub>2</sub>(trz)](BF<sub>4</sub>), *Eur. J. Inorg. Chem.*, 2018, **2018**, 429–434.
- 70 C. P. Slichter and H. G. Drickamer, Pressure-Induced Electronic Changes in Compounds of Iron, *J. Chem. Phys.*, 1972, **56**, 2142–2160.
- 71 M. Sorai and S. Seki, Phonon coupled cooperative low-spin <sup>1</sup>A<sub>1</sub> high-spin <sup>5</sup>T<sub>2</sub> transition in [Fe(phen)<sub>2</sub>(NCS)<sub>2</sub>] and [Fe(phen)<sub>2</sub>(NCSe)<sub>2</sub>] crystals, *J. Phys. Chem. Solids*, 1974, **35**, 555–570.
- 72 O. Roubeau, M. Castro, R. Burriel, J. G. Haasnoot and J. Reedijk, Calorimetric investigation of triazole-bridged Fe(II) spin-crossover one-dimensional materials: Measuring the cooperativity, *J. Phys. Chem. B*, 2011, **115**, 3003–3012.

